Available online at www.sciencedirect.com
ScienceDirect
Journal of Power Sources 161 (2006) 183–190
JOURNAL OF POWER SOURCES
www.elsevier.com/locate/jpowsour

Modeling techniques applied to the study of gas diffusion electrodes and proton exchange membrane biochemical fuel cells

Ruy Sousa Jr., Flávio Colmati, Ernesto Rafael Gonzalez *

Instituto de Química de São Carlos, Universidade de São Paulo, Av. Trabalhador Sãocarlense, 400, C.P. 780, 13560-970 São Carlos, SP, Brazil

Received 16 January 2006; received in revised form 7 March 2006; accepted 7 March 2006
Available online 14 June 2006

Abstract

Mathematical modeling has been extensively applied to the study and development of fuel cells. In this laboratory, modeling studies of gas diffusion electrodes and proton exchange membrane biochemical fuel cells are being developed. Regarding the modeling of usual physical systems, the available knowledge makes it possible to develop mechanistic models. For biochemical fuel cells, on the other hand, semi-empirical and empirical models can be used. In this work, there are three objectives: characterize a *phenomenological* model for a Pt–air cathode and perform appropriate simulations; characterize a *semi-empirical* model to predict the performance of a Pt–H_2/H_2O_2-peroxidase fuel cell; investigate the effectiveness of (*empirical*) neural networks to predict the performance of a Pt–H_2/O_2-peroxidase fuel cell. The mechanistic model of a Pt–air cathode developed here is based on proper material balances, on Fick's law of diffusion and on Tafel kinetics. It can provide details of the physical system (such as the limit of the one-phase regime). A semi-empirical model based on Michaelis–Menten kinetics, in turn, can predict the performance of a Pt–H_2/H_2O_2-peroxidase biochemical fuel cell. Artificial neural networks were capable of fitting the potential/current relationship of a Pt–H_2/O_2-peroxidase biochemical fuel cell.

Keywords: Fuel cell cathodes; Phenomenological model; Biochemical fuel cells; Semi-empirical model; Neural networks

1. Introduction

Mathematical modeling has been extensively applied to the study and development of fuel cells. Sousa and Gonzalez [1] reviewed the state-of-the-art regarding modeling of fuel cells with a polymer electrolyte membrane.

The optimal modeling approach differs for each application [1,2]. Empirical models, specific for each application and set of operating conditions, are useful tools to predict the cell performance. Mechanistic models, in turn, besides their predictive capability, also can provide a detailed description of the cell and its components. A mechanistic fuel cell model is based on transport phenomena and electrochemical relationships.

In this laboratory, modeling studies of gas diffusion electrodes and proton exchange membrane biochemical fuel cells are being developed. Regarding the modeling of usual physical systems, the available knowledge makes it possible to develop mechanistic models. For biochemical fuel cells, on the other hand, to which less phenomenological knowledge is available, empirical (and semi-empirical) models can be used. This work has three objectives: characterize a *phenomenological* model for a Pt–air cathode and perform appropriate simulations; characterize a *semi-empirical* model to predict the performance of a Pt–H_2/H_2O_2-peroxidase fuel cell; investigate the effectiveness of (*empirical*) neural networks to predict the performance of a Pt–H_2/O_2-peroxidase fuel cell.

2. Background

2.1. Computational fluid dynamics

Over the past decade or so, computational fluid dynamics (CFD) techniques have been used extensively to model fuel cells. CFD is based on the solution of phenomenological conservation equations (mass, momentum, species, ...

* Corresponding author. Tel.: +55 16 33739899; fax: +55 16 33739952.
E-mail address: ernesto@iqsc.usp.br (E.R. Gonzalez).

0378-7753/$ – see front matter © 2006 Elsevier B.V. All rights reserved.
doi:10.1016/j.jpowsour.2006.03.094

Nomenclature

A	constant (mM)
A_i	areas of control-volume faces (cm^2)
B	constant (mV)
C_k	species mass fraction
D_k	species diffusivity ($cm^2\ s^{-1}$)
D_k^{eff}	effective mass diffusivity ($cm^2\ s^{-1}$)
in_i	input signal
j	current density ($A\ cm^{-2}$ or $mA\ cm^{-2}$)
$j_0/C_{O_2,ref}$	constant in Tafel equation ($A\ cm^{-2}$)
j_{max}	maximum current density ($mA\ cm^{-2}$)
J_i	total flux in the i direction ($g\ cm^{-2}\ s^{-1}$)
k	permeability (cm^2)
K_m	Michaelis–Menten constant (mM)
L	cathode length (cm)
net_j	sum of the input weighted signal
R	resistance ($\Omega\ cm^2$)
S	substrate (peroxide) concentration (mM)
S_k	species source term ($g\ cm^{-3}\ s^{-1}$)
S_u	momentum source term ($g\ cm^{-2}\ s^{-2}$)
t	time (s)
tor	tortuosity
u	component of the velocity vector $\vec{u}$ in the x direction ($cm\ s^{-1}$)
$\vec{u}$	velocity vector ($cm\ s^{-1}$)
u_i	velocity in the i direction ($cm\ s^{-1}$)
v	component of the velocity vector $\vec{u}$ in the y direction ($cm\ s^{-1}$)
v_{max}	maximum reaction rate ($mol\ cm^{-3}\ s^{-1}$)
v_{MM}	reaction rate ($mol\ cm^{-3}\ s^{-1}$)
V_0	open circuit potential (V or mV)
w_{jb}	an off-set term
w_{ji}	weighted connections
x	x axis (cm)
x_i	ith axis (cm)
y	y axis (cm)
y_j	unit output

Greek letters

α	water transport coefficient
α_C	cathode transfer coefficient
Γ	diffusion coefficient ($g\ cm^{-1}\ s^{-1}$)
ε	porosity
η	overpotential (V or mV)
η_{net}	learning rate
μ^{eff}	effective viscosity ($g\ cm^{-1}\ s^{-1}$)
ρ	density ($g\ cm^{-3}$)
ϕ	dependent variable

(Eqs. (1a)–(1c))) on a computational grid by using either finite-difference, finite-volume or finite-element methodologies [3–5].

$$\frac{\partial(\varepsilon\rho)}{\partial t} = -\nabla\cdot(\varepsilon\rho\vec{u}) \tag{1a}$$

$$\frac{\partial(\varepsilon\rho\vec{u})}{\partial t} = -\nabla\cdot(\varepsilon\rho\vec{u}\vec{u}) - \varepsilon\nabla P + \nabla\cdot(\varepsilon\mu^{eff}\nabla\vec{u}) + S_u \tag{1b}$$

$$\frac{\partial(\varepsilon\rho C_k)}{\partial t} = -\nabla\cdot(\varepsilon\vec{u}\rho C_k) + \nabla\cdot(D_k^{eff}\rho\nabla C_k) + S_k \tag{1c}$$

where

$$S_u = -\frac{\mu}{k}\varepsilon^2\vec{u}\ \text{(diffusion layer)} \quad \text{and} \quad S_k \propto \frac{-jc}{nF}\ \text{(catalyst layer)}$$

2.2. Kinetics of enzyme-catalyzed reactions

It has been observed, regarding the kinetics of many enzyme-catalyzed reactions, that:

- kinetics is first order when the substrate concentration, S, is low;
- when the substrate concentration is high, reaction order is zero.

Those observations can be quantified through the Michaelis–Menten kinetics:

$$v_{MM} = \frac{v_{max}S}{K_m + S} \tag{2}$$

Briggs and Haldane [6] have provided a derivation of Eq. (2) with a rigorous mathematical analysis (although Henri as well as Michaelis and Menten also have provided their own theoretical explanations [6]). Regarding the kinetics associated with the reduction of peroxide by horseradish peroxidase (the most extensively studied peroxidase), a Michaelis–Menten-like equation arises (as a function of H_2O_2 concentration) when the concentration of reducing substrate is approximately constant [7]. Regarding the integration of electrochemistry and biotechnology, Bartlett et al. [8] fitted a Michaelis–Menten-type model (at a specific potential) for the current density (as a function of H_2O_2 concentration) associated with the horseradish peroxidase-catalyzed decomposition of H_2O_2.

2.3. Artificial neural networks (ANN's)

Multi-Layer Perceptron (MLP, also called feedforward) is a class of ANN's [9,10] extensively used. A MLP ANN consists of interconnected layers (input, hidden and output) of processing units (neurons). Neurons in adjacent layers are joined by weighted connections (w_{ji}). Each unit sums (net_j) the input weighted signal ($w_{ji}in_i$) and an off-set term (bias, w_{jb}):

$$net_j = \sum_{i=1}^{n} w_{ji}in_i + w_{jb} \tag{3}$$

A non-linear function evaluates net_j, producing the unit output (y_j). In most cases:

$$y_j = \frac{1}{1+\exp(-net_j)} \tag{4}$$

In the training process, the neural weights are adjusted, usually by using the "backpropagation algorithm" (in a back direction from output to input layer [11]). The change in weights is based on the gradient descent rule:

$$\Delta w_{ji} = -\eta_{\text{net}} \frac{\partial(\text{sum of squared errors})}{\partial w_{ji}} \quad (5)$$

Regarding the empirical modeling of polymer electrolyte membrane fuel cells Lee et al. [12] presented an ANN model as a practical alternative to analytical and empirical models of fuel cells. Ou and Achenie [13], in turn, showed that an ANN model was capable of simulating some effects for which there are currently no valid fundamental models available from the open literature.

3. Materials and methods

Empirical and semi-empirical models are data-based ones. Therefore, some experiments were carried out to provide the necessary data for the modeling of the biochemical cells.

The enzyme source was a material properly extracted (according to [14]) from the Brazilian zucchini squash *Cucurbita pepo*. After washing and drying, the vegetal tissue was peeled, homogenized in a liquefier (1 g of zucchini in 10 ml of water) and filtered. After the filtering, a proper quantity of active carbon was added to the solution. It was centrifuged (at 2000 rpm) and the supernatant was separated, frozen in liquid nitrogen and lyophilized to dryness. That extract from Brazilian zucchini was used in different ways for preparing the cathodes.

The adsorption procedure of a protein is relatively simple and extensively used. The enzyme can also be immobilized on a solid support through low energy bonds, such as van der Waals forces, hydrogen bridges and ionic bonds. Starting from the enzyme source, three kinds of electrodes were prepared. The enzyme was adsorbed (referred below as cathode condition 3 for neural network processing) and immobilized (referred below as cathode condition 2 for neural network processing) on a carbon tissue (PWB-3, Stackpole). Before depositing the enzyme, the carbon tissue was submitted to a treatment with nitric acid and properly washed with water purified in a milli-Q system. In the adsorption procedure, a piece of carbon tissue was immersed into the aqueous solution containing the enzymatic extract at a concentration of 15 mg ml^{-1}, and properly lyophilized. For immobilization, the dried tissue containing the adsorbed extract was immersed into a chloroform solution (Merck) containing 1 mM of dicyclohexylcarbodiimide (Aldrich) and properly dried in an airflow. Electrodes with the enzyme adsorbed on active carbon powder were also prepared (referred below as cathode condition 1 for neural network processing). In this case, the carbon powder was added to the enzyme extract for adsorption. An additional type of electrode can be prepared when the enzymes are immobilized by immersing the enzyme adsorbed on active carbon powder into a chloroform solution (Merck) containing 1 mM of dicyclohexylcarbodiimide (Aldrich), but no experiments in a single cell were performed using this kind of electrode.

In the single cell experiments a Pt/C electrode, containing 0.4 mg Pt cm^{-2}, was used. The anode was prepared by distributing the Pt catalyst on a carbon tissue containing carbon powder and Teflon® (Dupont).

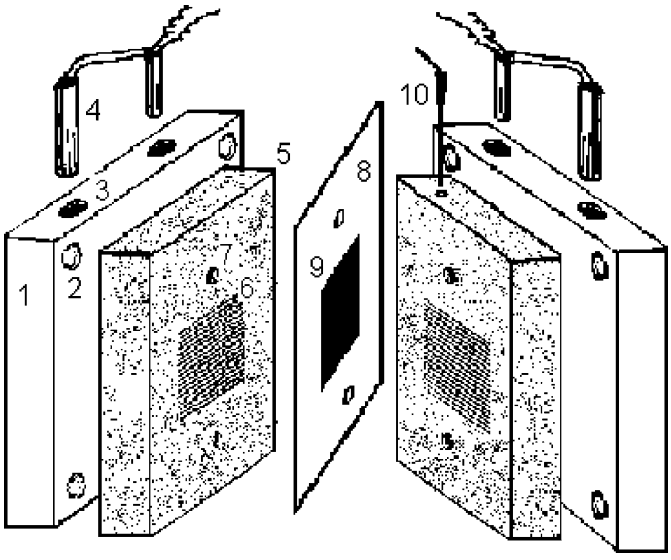

Fig. 1. Schematic diagram showing the components of a single polymer electrolyte membrane bio fuel cell: (1) aluminum plate; (2) screw input; (3) heaters input; (4) gas heaters (optional use); (5) graphite plate; (6) flow distributor; (7) fit guide; (8) membrane; (9) electrodes; (10) thermocouple.

3.1. Pt–H_2/H_2O_2-peroxidase biochemical fuel cell

Experiments in a single cell, with a (immobilized on a carbon tissue) Brazilian zucchini squash peroxidase cathode, were carried out. A Nafion® 117 membrane was used as the electrolyte. The Pt/C anode was hot pressed to the chosen membrane, and then the cathode was put into contact with it, since the enzymes cannot support high pressures.

Hydrogen was fed to the anode, while a 0.8 mM hydrogen peroxide solution was supplied to the cathode. Atmospheric pressure (1 atm) and room temperature (24 °C) were the working conditions. The cell voltage and the circulating current were measured with multimeters. Fig. 1 shows a schematic diagram of the cell (but gas heaters are not used for liquid feed).

3.2. Pt–H_2/O_2-peroxidase biochemical fuel cell

Twelve experiments were carried with the Brazilian zucchini squash peroxidase cathode in a single cell, using either a deposited enzyme on active carbon powder (named condition 1, only to be distinguished from the other conditions), or immobilized on a carbon tissue (named condition 2) or deposited on a carbon tissue (named condition 3). A Nafion® 117 membrane was used as the electrolyte. The Pt/C anode was hot pressed to the membrane, while the cathodes were put into contact with it.

Hydrogen was fed to the anode, while oxygen was supplied to the cathode. Adequate pressure (1 atm) and temperatures (24 °C and 35 °C) were selected. The cell voltage was measured as a function of the current. Fig. 1, again, shows a scheme of the cell.

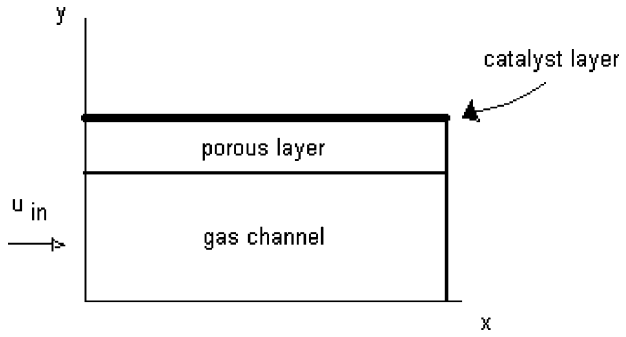

Fig. 2. Scheme of a porous cathode of a PEMFC.

4. Results and discussion

4.1. Pt–air cathode

The mathematical model (within the CFD framework) of a Pt–air cathode (Fig. 2; Eq. (6)) developed here is based on species mass fraction equations (oxygen, water vapor and inert gas), since one hypothesis was considered: negligible velocity field in the porous layer, where gas diffusion is the dominant transport mechanism, and fully developed plug-flow field in the gas channel.

$$\frac{\partial(\varepsilon\rho C_k)}{\partial t} = -\nabla\cdot(\varepsilon\vec{u}\rho C_k) + \nabla\cdot(\varepsilon^{\text{tor}}\rho D_k \nabla C_k) \tag{6}$$

$0 < y <$ channel height:

$$u|_{x=0} = u_{\text{in}}, \quad v|_{x=0} = 0,$$
$$C_{\text{H}_2\text{O}}|_{x=0} = 0.015, \quad C_{\text{O}_2}|_{x=0} = 0.23, \quad C_{\text{inert}}|_{x=0} = 0.755$$

Channel height $< y <$ total height:

$$u|_{x=0} = 0, \quad v|_{x=0} = 0,$$
$$\left(\frac{\partial(C_{\text{H}_2\text{O}})}{\partial x}\right)\bigg|_{x=0} = 0, \quad \left(\frac{\partial(C_{\text{O}_2})}{\partial x}\right)\bigg|_{x=0} = 0, \quad \left(\frac{\partial(C_{\text{inert}})}{\partial x}\right)\bigg|_{x=0} = 0$$
$$u|_{x=L} = 0, \quad v|_{x=L} = 0,$$
$$\left(\frac{\partial(C_{\text{H}_2\text{O}})}{\partial x}\right)\bigg|_{x=L} = 0, \quad \left(\frac{\partial(C_{\text{O}_2})}{\partial x}\right)\bigg|_{x=L} = 0, \quad \left(\frac{\partial(C_{\text{inert}})}{\partial x}\right)\bigg|_{x=L} = 0$$

$0 < x <$ cell length:

$$u|_{y=0} = u_{\text{in}}, \quad v|_{y=0} = 0,$$
$$\left(\frac{\partial(C_{\text{H}_2\text{O}})}{\partial y}\right)\bigg|_{y=0} = 0, \quad \left(\frac{\partial(C_{\text{O}_2})}{\partial y}\right)\bigg|_{y=0} = 0, \quad \left(\frac{\partial(C_{\text{inert}})}{\partial y}\right)\bigg|_{y=0} = 0$$

Table 1
Values of the parameters used in the simulation of the Pt–air cathode

Water vapor diffusivity, $D_{\text{H}_2\text{O}}$ ($\text{cm}^2\,\text{s}^{-1}$)	0.32
Oxygen diffusivity, D_{O_2} ($\text{cm}^2\,\text{s}^{-1}$)	0.25
Inert diffusivity, D_{inert} ($\text{cm}^2\,\text{s}^{-1}$)	0.25
Diffusion layer porosity, ε	0.3
Diffusion layer tortuosity, tor	1.1
Water transport coefficient, α	0.2
Constant in Tafel equation, $j_0/C_{\text{O}_2,\text{ref}}$ ($\text{A}\,\text{cm}^{-2}$)	0.2×10^{-4}
Cathode transfer coefficient, α_{C}	1.2
Open circuit potential, V_0 (V)	1.1
Channel height (cm)	0.075
Gas diffusion layer height (cm)	0.045
Cathode length, L (cm)	2
Water vapor mass fraction at the inlet, $C_{\text{H}_2\text{O}}\big\vert_{x=0}$	0.015
Oxygen mass fraction at the inlet, $C_{\text{O}_2}\big\vert_{x=0}$	0.23
Inert mass fraction at the inlet, $C_{\text{inert}\vert x=0}$	0.755
Air velocity at the inlet, u_{in} ($\text{cm}\,\text{s}^{-1}$)	35
Temperature, T (°C)	80 (353 K)
Pressure, P (atm)	1

Membrane cathode interface (where the oxygen reduction reaction takes place):

$$u|_{y=\text{total height}} = 0, \quad v|_{y=\text{total height}} = 0,$$
$$-\varepsilon^{\text{tor}} D_k \left(\frac{\partial(\rho C_{\text{H}_2\text{O}})}{\partial y}\right)\bigg|_{y=\text{total height}} = \frac{-M_{\text{H}_2\text{O}}(1+2\alpha)j}{2F}$$
$$-\varepsilon^{\text{tor}} D_k \left(\frac{\partial(\rho C_{\text{O}_2})}{\partial y}\right)_{y=\text{total height}} = \frac{M_{\text{O}_2} j}{4F}$$
$$j = \left(\frac{j_0}{C_{\text{O}_2,\text{ref}}}\right) C_{\text{O}_2}\ \exp\left(\frac{-\alpha_{\text{c}} F\eta}{RT}\right)$$

Other considerations are: steady-state operation, Fick's diffusion mechanism and Tafel kinetics, to describe the current density along the membrane/cathode interface (as a boundary condition, instead of as a source term). Table 1 shows the values of the parameters used in the simulation.

The solution of conservation equations on a computational grid was performed by starting from the solver implemented into the free-software MFIX [15]. Briefly, the essence of partial differential equations solvers is the discretization of equations in appropriate control volumes. For the integration of Eq. (6) over

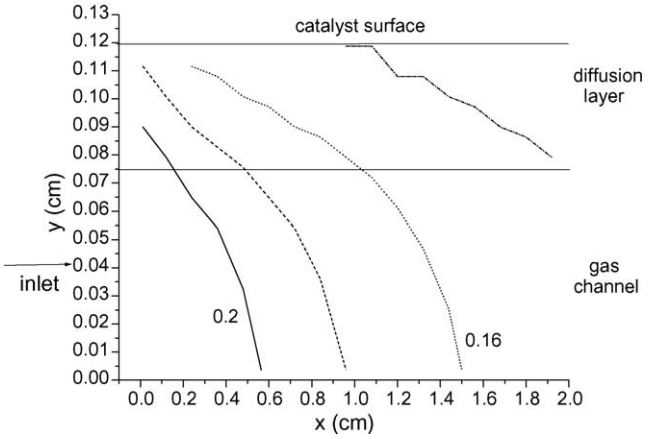

Fig. 3. Oxygen mass fraction contours in a Pt–air cathode at 0.41 A cm^{-2} and 0.81 V.

a control volume, it is convenient to combine the convection and diffusion fluxes:

$$J_i = \rho u_i \phi - \Gamma \frac{\partial \phi}{\partial x_i} \tag{7}$$

$$\frac{\partial}{\partial t}(\rho\phi) + \frac{\partial J_i}{\partial x_i} = 0 \tag{8}$$

$$(\rho_p \phi_p - \rho_p^0 \phi_p^0)\left(\frac{\Delta \text{Area}}{\Delta t}\right) + J_e A_e - J_w A_w + J_n A_n - J_s A_s = 0 \tag{9}$$

where ϕ is the dependent variable C_k ($k = H_2O$, O_2, inert) and $\Gamma = \varepsilon^{\text{tor}-1}\rho D_k$.

For steady-state conditions, the first term in Eq. (9) vanishes. Certain approximations to the total flux expression have been presented [16,17]. If the fluxes in Eq. (9) are written in terms of the proper expressions, a system of algebraic equations arises when all points in the grid are considered.

Figs. 3–8 show the results of the simulations of the Pt–air cathode. They show the mass fraction profiles of oxygen and water vapor (the mass fraction of inert gas is simply $(1 - C_{H_2O} - C_{O_2})$) in three different average current densities (and the associated potentials). It is possible to observe the oxygen consumption with the increase in current density as well as the increase in water formation. In particular, at a current density of 0.83 A cm^{-2} (cathode potential 0.77 V versus SHE), it is possible to observe the limit of one-phase regime (Fig. 8), i.e., when the water vapor density at the membrane/cathode inter-

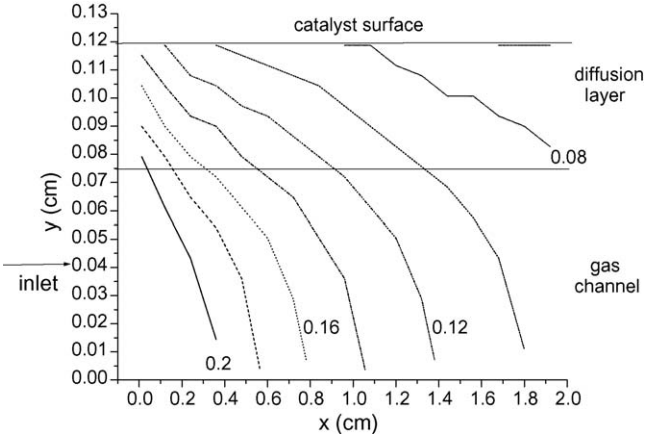

Fig. 4. Oxygen mass fraction contours in a Pt–air cathode at 0.69 A cm^{-2} and 0.78 V.

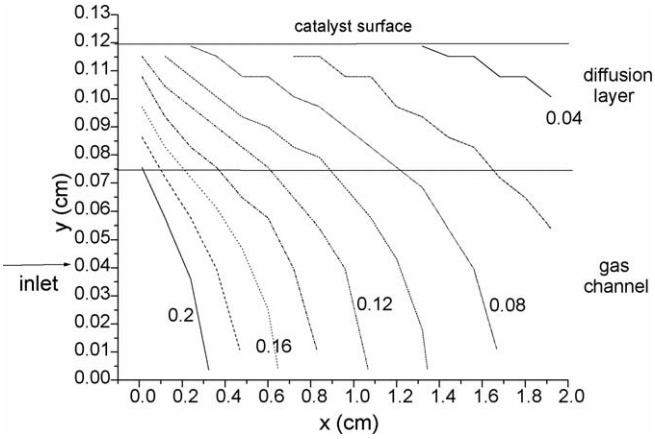

Fig. 5. Oxygen mass fraction contours in a Pt–air cathode at 0.83 A cm^{-2} and 0.77 V.

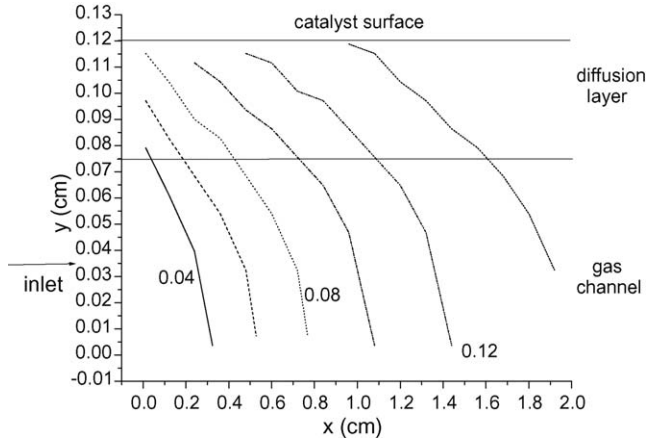

Fig. 6. Water mass fraction contours in a Pt–air cathode at 0.41 A cm^{-2} and 0.81 V.

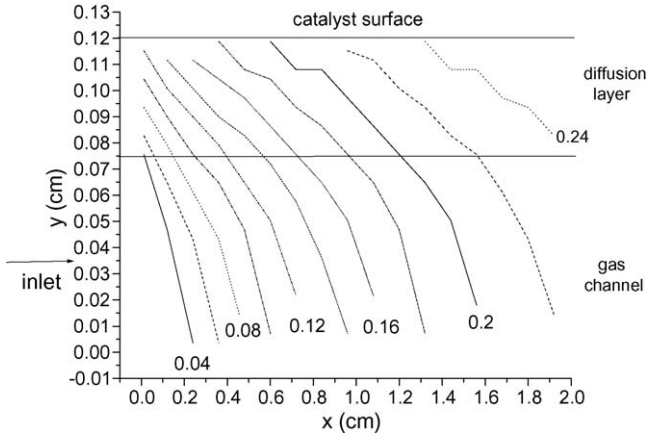

Fig. 7. Water mass fraction contours in a Pt–air cathode at 0.69 A cm^{-2} and 0.78 V.

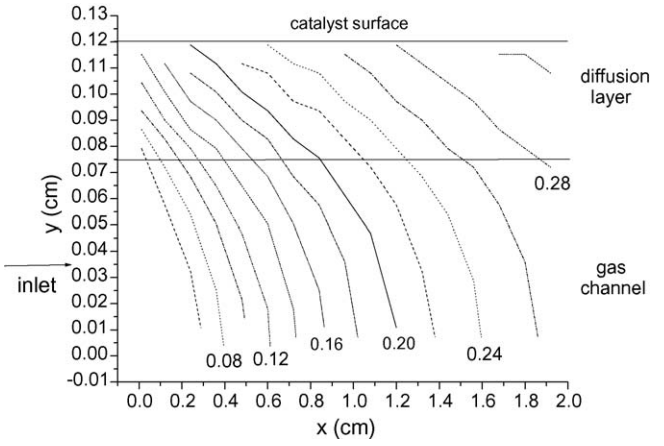

Fig. 8. Water mass fraction contours in a Pt–air cathode at 0.83 A cm^{-2} and 0.77 V.

face reaches the saturation value associated with the operating temperature (corresponding to $C_{H_2O} \approx 0.3$).

With a further increase in the current density, a two-phase zone will form, and a two-phase model will be necessary.

4.2. Pt–H_2/H_2O_2-peroxidase biochemical fuel cell

The semi-empirical model of a Pt–H_2/H_2O_2-peroxidase fuel cell developed here is based on a Michaelis–Menten-like equation for the current density (as a function of H_2O_2 concentration (S in Eq. (10)) associated with the peroxidase-catalyzed decomposition of H_2O_2 and using it to model the cell performance (Eq. (11)).

$$j = \frac{j_{max} S}{K_m + S} \tag{10}$$

with

$$K_m = A \exp\left(\frac{\eta}{B}\right)$$

$$V = V_0 - Rj + B \ln\left[\frac{S}{A}\left(\frac{j_{max}}{j} - 1\right)\right] \tag{11}$$

Fitted parameters by using experimental data, Eq. (11) and Levenberg–Marquardt algorithm [18] implemented into Microcal Origin® were (for $V_0 = 700$ mV, $S = 0.8$ mM and considering $j_{max} = 1.5$ mA cm^{-2}): $B = 123$ mV, $A = 45$ mM.

Fig. 9 shows graphically the predictions of the Michaelis–Menten-like equation for the current density as a function of the H_2O_2 concentration. Fig. 10 shows experimental and model potential/current relationships for the Pt–H_2/H_2O_2-peroxidase fuel cell. A very good agreement is observed between experimental and model values.

4.3. Pt–H_2/O_2-peroxidase biochemical fuel cell

The empirical neural network model of a Pt–H_2/O_2-peroxidase fuel cell developed here maps three input variables—temperature, current density and cathode conditions, i.e., with enzymes deposited on active carbon powder (1), immobilized

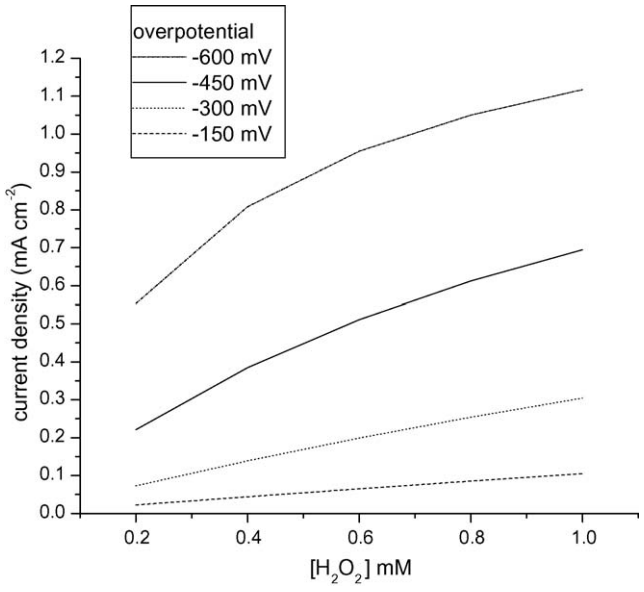

Fig. 9. Current density vs. H_2O_2 concentration for a peroxidase cathode.

on a carbon tissue (2) or deposited on a carbon tissue (3), into and output space associated with the cell potential (Fig. 11).

Regarding the training process, neural weights were adjusted by using the "backpropagation algorithm" implemented into an in-house software (original version by CAO Nascimento, DEQ-EPUSP, modified by AJG Cruz, DEQ-UFSCar, modified by R. Sousa Jr., and used previously in the characterization of a neural model for whey protein hydrolysis [19]).

Fig. 12 shows the learning accuracy associated with the neural network. The meaning of obtaining a neural versus experimental relationship close to $f(x) = x$ is that the neural network responses are very accurate.

Figs. 13–15, in turn, show experimental and neural potential/current relationships for the Pt–H_2/O_2-peroxidase fuel cells (training data points, except where indicated as validation

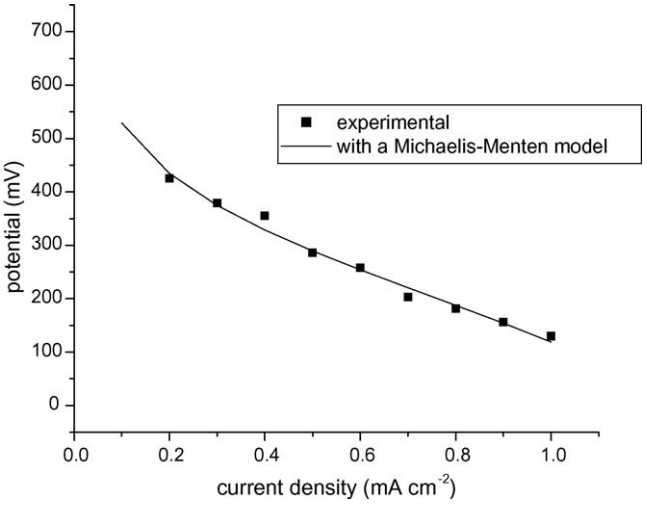

Fig. 10. Potential/current relationship for a Pt–H_2/H_2O_2-peroxidase fuel cell. $T = 24$ °C, $p(H_2) = 1$ atm, [H_2O_2] = 0.8 mM.

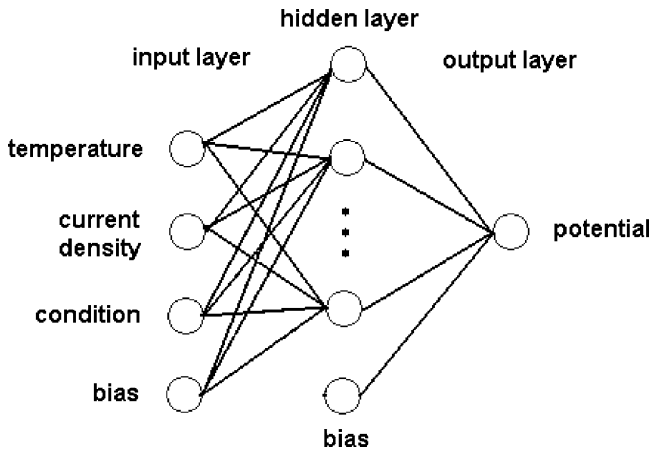

Fig. 11. Schematic diagram of the artificial neural network.

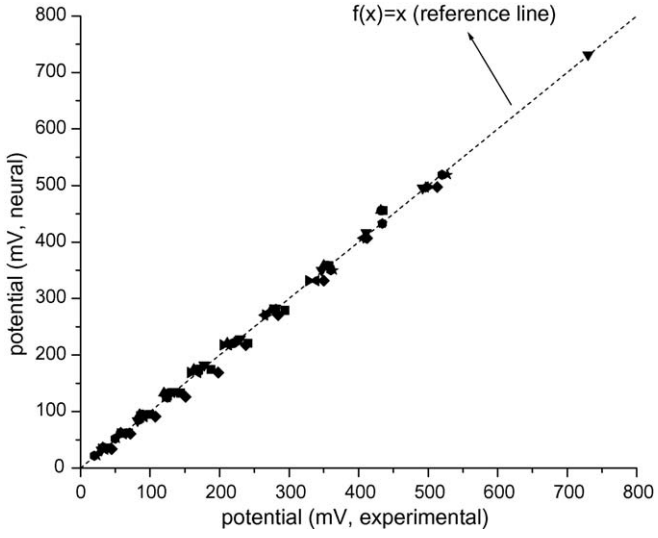

Fig. 12. Accuracy test associated with the neural network.

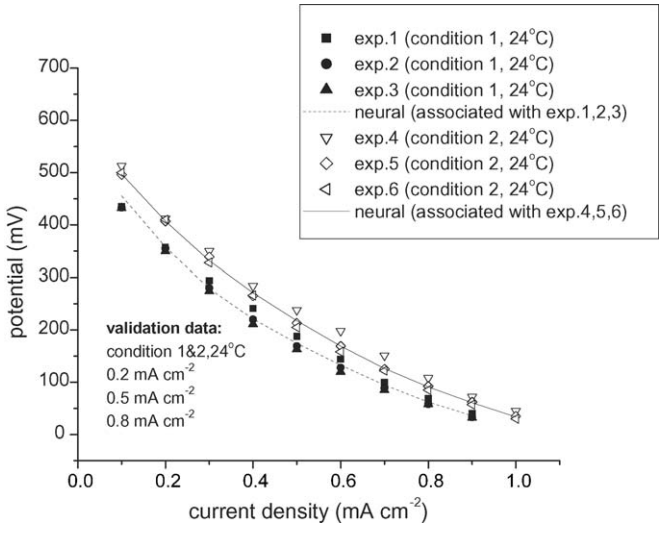

Fig. 13. Experimental and neural potential/current relationships for a Pt–H_2/O_2-peroxidase fuel cell. Cathode preparation conditions 1 and 2.

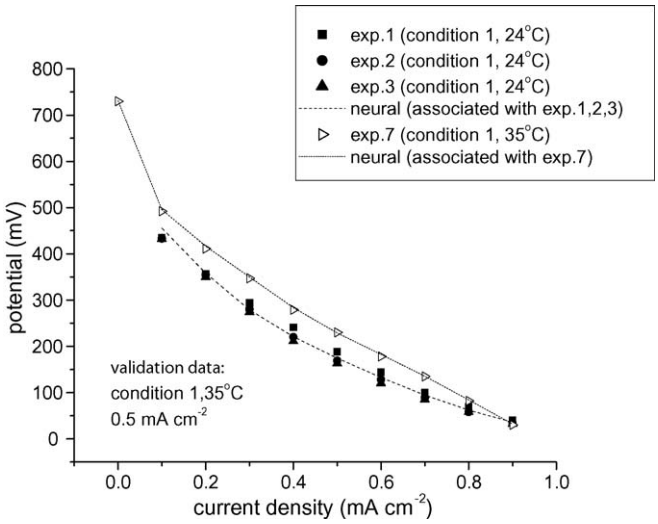

Fig. 14. Experimental and neural potential/current relationships for a Pt–H_2/O_2-peroxidase fuel cell. Cathode preparation condition 1 and different temperatures.

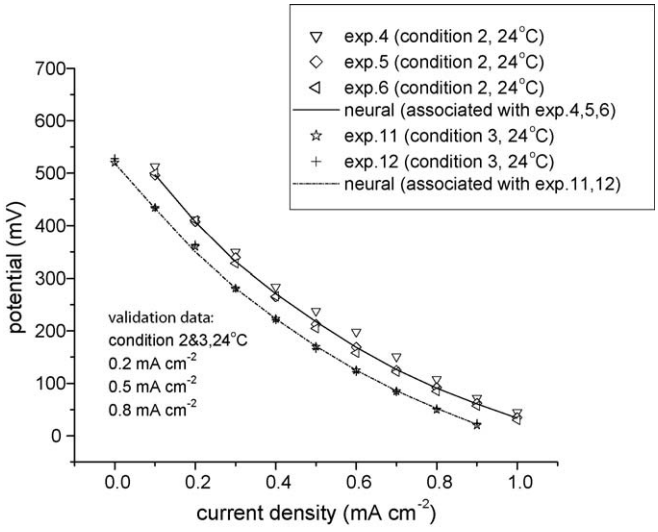

Fig. 15. Experimental and neural potential/current relationships for a Pt–H_2/O_2-peroxidase fuel cell. Cathode preparation conditions 2 and 3.

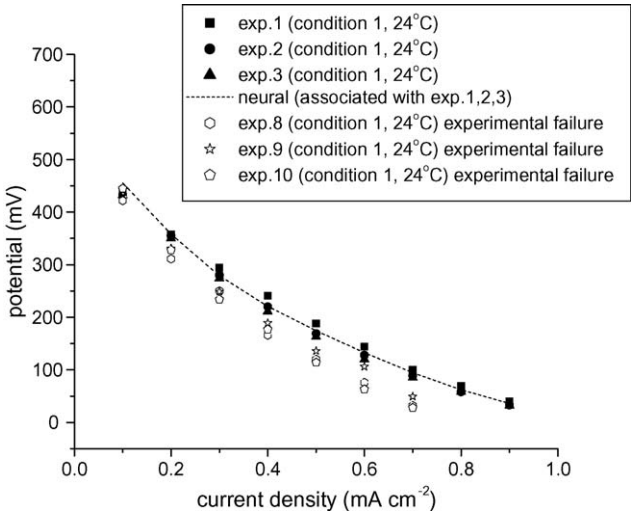

Fig. 16. Experimental and neural potential/current relationships for a Pt–H_2/O_2-peroxidase fuel cell. Failure detection.

points). It is possible to observe a very good agreement between experimental and neural values. In Fig. 16, an additional feature of artificial neural networks is presented, failure detection: under the best conditions (experiments 1–3), the peroxidase electrode was pre-humidified; in experiments 8–10, however, pre-humidification was not performed and the performance is lower than the neural prediction. This indicates a failure in the experimental procedure.

5. Conclusions

The main conclusions of this work may be summarized as follows:

A mechanistic model was developed for a Pt–air cathode, which can provide details of the physical system (such as the limit of the one-phase regime).
A semi-empirical model based on Michaelis–Menten kinetics is adequate to predict the performance of a Pt–H_2/H_2O_2-peroxidase biochemical fuel cell.
Artificial neural networks were capable of fitting the potential/current relationships of Pt–H_2/O_2-peroxidase biochemical fuel cells.

Acknowledgements

R. Sousa Jr. thanks FAPESP for a post-doctoral scholarship. Thanks are also due to FAPESP and CNPq for financial support. Finally, the authors would like to thank Dr. S.A. Yoshioka for the bio-electrode preparation.

References

[1] R. Sousa Jr., E.R. Gonzalez, J. Power Sources 147 (2005) 32–45.
[2] K. Haraldsson, K. Wipke, J. Power Sources 126 (2004) 88–97.
[3] S. Mazumder, J.V. Cole, J. Electrochem. Soc. 150 (2003) A1503–A1509.
[4] S. Um, C.Y. Wang, K.S. Chen, J. Electrochem. Soc. 147 (2000) 4485–4493.
[5] S.V. Patankar, Numerical Heat Transfer and Fluid Flow, Hemisphere Publishing Corporation, USA, 1980.
[6] J.E. Bailey, D.F. Ollis, Biochemical Engineering Fundamentals, McGraw Hill Book Company, USA, 1986.
[7] J. Everse, K.E. Everse, M.B. Grisham, Peroxidases in Chemistry and Biology, vol. II, CRC Press, USA, 1991.
[8] P.N. Bartlett, D. Pletcher, J. Zeng, J. Electrochem. Soc. 144 (1997) 3705–3710.
[9] O. Nelles, Nonlinear System Identification, Springer-Verlag, Berlin/Heidelberg/USA, 2001.
[10] F. Scarselli, A.C. Tsoi, Neural Netw. 11 (1998) 15–37.
[11] D.E. Humelhart, G.E. Hinton, R.J. Williams, Nature 323 (1986) 533–536.
[12] W.Y. Lee, G.G. Park, T.H. Yang, Y.G. Yoon, C.S. Kim, Int. J. Hydrogen Energy 29 (2004) 961–966.
[13] S. Ou, L.E.K. Achenie, J. Power Sources 140 (2005) 319–330.
[14] O. Fatibello-Filho, I. Vieira, Química Nova 23 (2002) 455–464.
[15] M. Syamlal, W. Rogers, T.J. O'Brien, MFIX Documentation—Theory Guide, U.S. Department of Energy, Office of Fossil Energy, Morgantown Energy Technology Center, USA, 1993.
[16] M. Syamlal, MFIX Documentation—Numerical Technique, U.S. Department of Energy, Office of Fossil Energy, Federal Energy Technology Center, USA, 1998.
[17] W.J. Minkowycz, E.M. Sparrow, G.E. Schneider, R.H. Pletcher, Handbook of Numerical Heat Transfer, John Wiley & Sons, USA, 1988.
[18] D.W. Marquardt, J. Soc. Ind. Appl. Math. 11 (1963) 431–441.
[19] R. Sousa Jr., Inteligência Computacional Aplicada à Automação da Hidrólise Enzimática de Soro de Queijo em Reator Contínuo, Ph.D. Dissertation, Universidade Federal de São Carlos, Brazil, 2003.